Korean J. Chem. Eng., 32(12), 2524-2533 (2015)
DOI: 10.1007/s11814-015-0067-1

pISSN: 0256-1115
eISSN: 1975-7220

The effect of chemical modification of SiO_2 nanoparticles on the nanofiltration characteristics of polyamide membrane

Nasim Rakhshan and Majid Pakizeh†

Department of Chemical Engineering, Faculty of Engineering, Ferdowsi University of Mashhad,
P. O. Box 9177948974, Mashhad, Iran
(*Received 16 December 2014 • accepted 3 April 2015*)

Abstract−This study presents the synthesis and characterization of oleic acid (OA)-modified silica/polyamide (PA) nanocomposite membranes. The thin film composite (TFC) polyamide was prepared with M-phenylendiamine (MPD) and trimesoyl chloride (TMC) via interfacial polymerization over porous polysulfone. Five different thin film nanocomposite (TFN) membranes were fabricated by dispersing OA-modified silica nanoparticles in TMC solution. Chemical and thermal properties, surface morphology, roughness, film thickness and hydrophilicity of synthesized membranes were characterized by ATR-IR, TGA, FESEM, AFM, TEM and contact angle analysis. The results showed that incorporating OA-modified silica into thin film layer improved chemical and physical properties of nanocomposite membranes. The effects of modification of nano silica on pure water flux and $MgSO_4$ rejection were investigated. OA-modified silica/PA membranes showed higher pure water flux in comparison with neat polyamide TFC membrane but lower than unmodified silica/PA membrane; while significant increase in salt rejection was exhibited for OA-modified silica/PA membranes. The maximum rejection for OA-modified and unmodified nanocomposite membrane was obtained about 98.7% and 95.2%, respectively.

Keywords: Nanocomposite Membrane, Oleic Acid Modified Silica, Polyamide, Interfacial Polymerization

INTRODUCTION

Application of thin film composite (TFC) membranes is increasingly recognized as one of the most popular forms of membrane separation processes for water treatment and brackish portable water. Many literature reports support polyamide membrane performance as the best TFC desalination membrane [1-5]. These asymmetric TFC membranes are composed of a top thin polyamide film coated over a porous polysulfone support membrane that is further reinforced by a non-woven polyester fabric. The active layer is usually made via interfacial polymerization of m-phenylenediamine (MPD) in aqueous phase and trimesoyl chloride (TMC) in organic phase [6-8]. For TFC membrane, the ultra-thin top layer is the key factor for determining the total properties of composite membrane, such as surface morphology, roughness, hydrophilicity, and thermal stability. Although polyamide thin film membranes have been used for water treatment in recent years, they require additional improvement to optimize their chemical-physical properties and performance. The use of inorganic nanoparticles as an additive to enhance top layer performance is now commercially carried out, and this new type of membrane is called a thin film nanocomposite (TFN) [9-14].

TFN membranes have produced new classes of desalination membranes, whose applications to water purification need more exploration. Recently, numerous reports on nanocomposite membranes have demonstrated the development of separation performance, permeability, selectivity, stability, or anti-fouling properties [15-19].

However, in the composite systems of mixed matrix membranes, there is a phase separation between the polymer (organic phase) and nano scale particles (inorganic phase). Furthermore, inorganic nanoparticles are very easy to agglomerate in polymeric matrix and show poor dispersion capacity in organic medium [20]. If the interactions between nanoparticles are stronger than that of between polymer molecules and nanoparticles, the nanoparticles agglomerate together to form some domains in micrometer sizes. The hydrophilic nature of silica arising from the hydroxyl group (-OH) on the silica surface brings about the nanoparticles to be easily agglomerated due to hydrogen bonding of hydroxyl groups and hardly dispersible in organic solvent and polymer matrix [21,22]. For example Namazi et al. reported poor compatibility between PPBI and silica nanoparticles and insignificant homogeneity of the PPBI/SiO_2 membranes [23]. To resolve these problems, the inorganic particles are treated with a surface agent or organic compounds to improve the affinity between the inorganic and the polymer phases [9]. Macromolecules can be adsorbed on the surface of nanoparticles and can be replaced with the surface OH groups on nanoparticles. When a macromolecule is attached to the surface of nanoparticles, it produces a thin organic shell on the surface of nanoparticles. The interactive exclusion and steric repulsions effect of this shell can reduce the agglomeration of nanoparticles [24-26]. The modified nanoparticles can be dispersed stably in organic solvents when high-weight hydrocarbons are used as the surface modification agent [27]. In addition, the hydrophobic long alkyl chains on the surface of particles improve the affinity capacity of nanoparti-

†To whom correspondence should be addressed.
E-mail: pakizeh@um.ac.ir

cles in organic phase [20].

In the present work, a novel SiO_2/PA nanocomposite membrane was fabricated using modified silica nanoparticles which were functionalized by oleic acid (OA). The modified silica was incorporated into polyamide thin film membrane during the polymerization process, and finally improved parameters were established. The surface structure and other properties of the prepared nanocomposite membranes were investigated using field emission scanning electron microscopy (FESEM), attenuated total reflectance infrared spectroscopy (ATR-IR), transmission electron microscopy (TEM), contact angle and atomic force microscopy (AFM). In addition, the pure water flux and salt rejection of OA-modified silica/polyamide nanocomposite membranes were compared with unmodified silica/polyamide membranes.

MATERIALS AND METHODS

1. Chemicals

Polysulfone (PSf) beads (BASF, Germany), N-methyl pyrrolidone (NMP) (Sigma-Aldrich, USA) were used to provide support membrane. M-phenylendiamine (MPD) (Sigma-Aldrich, USA) and Trimesoyl chloride (TMC) (Sigma-Aldrich, USA) were used as aqueous and organic monomers in polyamide thin film formation. n-Hexan (Merck, Germany) was the organic solvent selected for preparing the TMC solution. A commercial form of nano silica with diameters in the range of 15 to 30 nm was purchased from Degussa. Oleic acid and 2-propanol (Merck, Germany) were used for modification of nano silica. $MgSO_4 \cdot 7H_2O$ (Merck, Germany) was prepared for feed solution.

2. Modification of Nano Silica with Oleic Acid

To prepare the OA-modified silica nanoparticles, 1 g oleic acid (OA) was mixed with 100 ml n-Hexan. Then, 1 g nano silica particles was added and stirred at 60 °C for 4 h. The solution was then filtered and washed thoroughly with 2-propanol and de-ionized water. Finally, modified silica was dried at 100 °C in an oven for 24 h.

3. TFN Membrane Preparation

The support UF membrane was fabricated by using the phase inversion technique. 17% polysulfone (PSf) was prepared by dissolving PSf beads into N-methyl pyrrolidone (NMP) and stirred vigorously at 20 °C for 24 h. Next, the casting solution was spread via casting bar over a polyester non-woven fabric support previously taped to a glass plate. The glass plate was immediately immersed in a deionized water bath at room temperature. After several minutes, the formed PSf porous support layer was separated from the glass plate, washed thoroughly with deionized water several times and stored in fresh deionized water at 5 °C.

Polyamide thin film was formed via interfacial polymerization atop the hand-cast PSf porous membrane as support layer. The support membrane was immersed in a 2.0 (w/v)% aqueous solution of MPD for 2 min. Excess MPD solution was then removed from the support membrane surface by using a rubber roller. The MPD saturated membrane was placed in dry air for 2 min as lag time to let MPD diffuse the membrane, then immersed into a 0.1 (w/v)% TMC solution in n-hexan for 1 min. After the polymerization period, the fabricated TFC membrane was dried in an oven at 70 °C for 10 min to remove excess organic solvent.

Table 1. Composition of TMC solution for the nanocomposite membranes

Sample	Silica/TMC (w/v)%
S0 (neat PA)	0
S1	0.033
S2	0.167
S3	0.33
S4	1.67
S5	3.33

To fabricate nanocomposite membrane, an appropriate amount of the silica nanoparticles (0.033-3.33 (w/v)%) was added into the 0.1 (w/v%) solution of TMC in n-hexane. After 1 h of vigorous stirring and 15 min sonication, a uniform and homogeneous solution was obtained. The polymerization step is like the above process. The prepared silica-polyamide composite membrane was finally cured at 70 °C for 10 min. The silica loading present in the TMC solution is shown in Table 1.

4. Membrane Characterization

The surface morphology and cross section of porous PSf support were observed by SEM (LED 1450 VP microscope, Germany). PA composite and modified silica/PA nanocomposite membranes morphologies were observed with an FESEM (TESCAN). The cross section structure of prepared TFC and TFN membranes was examined by TEM. To prepare the samples, without a polyester layer, they were stained with a 2% osmium tetraoxide (OsO_4) aqueous solution at room temperature for 4 h, washed with deionized water, dried and embedded in epoxy resin, and finally cured in an oven at 60 °C for 48 h. Embedded membranes were sliced with an ultramicrotome and placed on copper grids. TEM images were observed by a CM120 instrument (Philips, Holland) at an accelerating voltage of 100 KV. An ATR-IR instrument was used to characterize the chemical structure of membranes and measure approximate thickness of the thin polyamide films. A Thermo Nicolet Nexus 100 ATR-IR coupled with a ZnSe crystal at 45° operating angle was used. The film thicknesses can be approximated based on the absorbance values of the C-N polyamide band according to the following equation [2]:

$$\ln\left[\frac{A_t}{A_0}\right] = -\frac{2t}{d_p} \tag{1}$$

where, t (nm) is the thickness of polyamide layer, A_t and A_0 are the intensities of polyamide and support layer, respectively, and d_p (μm) is the depth of penetration of the beam into the sample varying with the wavelength (λ) and approximate as follows:

$$d_p = \frac{\lambda}{2\pi n_1\left(\sin^2\theta - \left(\frac{n_2}{n_1}\right)^2\right)^{1/2}} \tag{2}$$

where, λ (cm^{-1}) is the wavelength, θ is the beam angle; n_1 and n_2 are the refractive indexes of ZnSe crystal and sample.

The surface roughness of nanocomposite membranes was measured by atomic force microscopy (AFM) on Easyscan 2 Flex AFM (Nanosurf, Switzerland). AFM images were taken on five separate

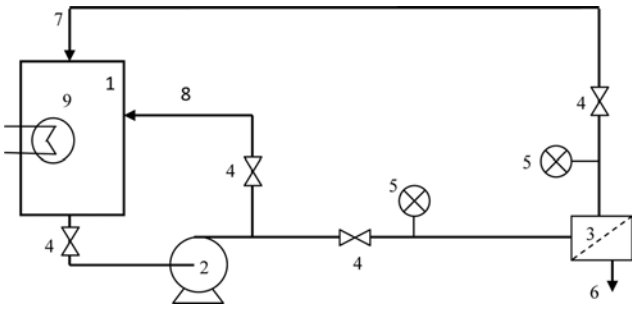

Fig. 1. The schematic diagram of cross flow system.

1. Feed tank	4. Valve	7. Retentate flow
2. Pump	5. Barometer	8. Bypass
3. Filtration cell	6. Permeate flow	9. Cooling system

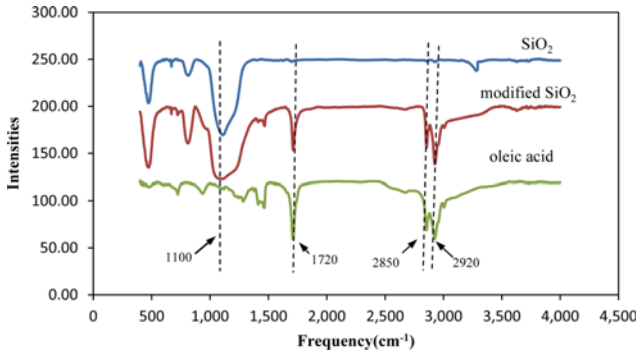

Fig. 2. FTIR spectra of oleic acid, unmodified silica and OA-modified silica.

occasions of each sample and average values were reported. Sessile drop contact angles of deionized water were measured on membrane samples in an environmental chamber mounted to a contact angle OCA15 plus goniometr (Dataphisics, CA). The equilibrium values were taken as the averages of left and right plateau contact angles. The reported data are the mean value of three equilibriums, which were obtained for each sample. The TGA instrument used for thermal analysis consisted of a TGA-50 model (Shimadzu, Japan). The thin film polyamide layer on the PSf support layer was extracted from the polyester. About 3 mg of samples was taken and heated from room temperature to about 900 °C at a heating rate of 10 °C/min.

5. Membrane Separation Performance

Pure water flux and salt rejection of nanocomposite membranes were determined by a stainless steel cross flow filtration setup with an effective membrane area of 9.62 cm^2 (Fig. 1). The permeation experiments were at room temperature and pressure of 0.8 MPa. Pure water flux, J_w (m^3/m^2s) was calculated by measuring the volume of permeate solution through the membrane per unit time according to the following equation:

$$J_w = \frac{Q_p}{A_m} \tag{3}$$

where, Q_p (m^3/s) is the permeate water flow rate and A_m (m^2) is the effective membrane area.

The water permeability coefficient, L_p (m^3/m^2 s Pa) was extracted directly from the water flux and the applied pressure according to:

$$L_p = \frac{J_w}{\Delta p} \tag{4}$$

The salt rejection was evaluated using standard aqueous feed containing 2,000 ppm $MgSO_4$ at 25 °C. Observed solute rejection was measured as follows:

$$X_s = \left(1 - \frac{C_p}{C_f}\right) \tag{5}$$

where, C_p and C_f are the solute concentrations in the permeate and feed solution, respectively. The influence of solute concentration polarization on the observed rejection was assumed negligible, due to small effective surface of membrane. The pore size of membranes was estimated using the exclusion model from the following equation [3]:

$$X_s = [\lambda(2-\lambda)]^2, \quad \lambda = \frac{r_s}{r_p} \tag{6}$$

where, r_p is the pore radius and r_s is the solute radius assumed for $MgSO_4$.

RESULTS AND DISCUSSION

1. Characterization of Modified Silica Nano Particles

The surface groups of silica nano particles before and after modification by oleic acid were characterized by FTIR. The OA spectrum in Fig. 2 indicates the long alkyl chain peaks at 2,920 and 2,850 cm^{-1} and COOH peak at 1,720 cm^{-1} [20]. These peaks are seen in the modified sample spectrum when compared to an unmodified sample. The strength of peak at 3,230 cm^{-1} corresponding to OH on the surface of the silica nanoparticles decreases in OA-modified silica curve. Thus, it can be concluded that the COOH has reacted with OH on the surface of nanosilica and the product is carboxylate. The appearance of these peaks on the surface of modified silica implies that functional groups of OA have been successfully absorbed on the silica surface due to electrostatic interactions. A proposed structural model for oleic acid modified silica nanoparticles is illustrated in Fig. 3.

2. Characterization of TFC and TFN Membranes

The ATR-FTIR spectra for PA and five nanocomposite membranes are shown in Fig. 4. The spectra reveal both effective thin layer of PA and PSf sub-layer because the IR beam penetration depth exceeds the thickness of the polyamide layer. The IR spectra

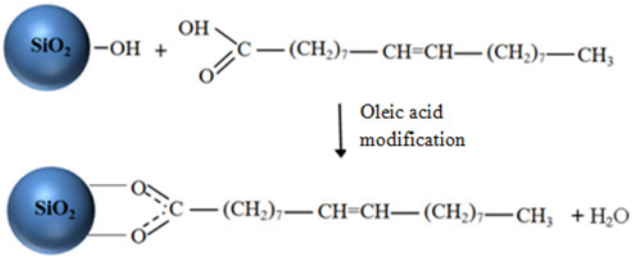

Fig. 3. Proposed mechanism of reaction between SiO_2 nanoparticles and oleic acid.

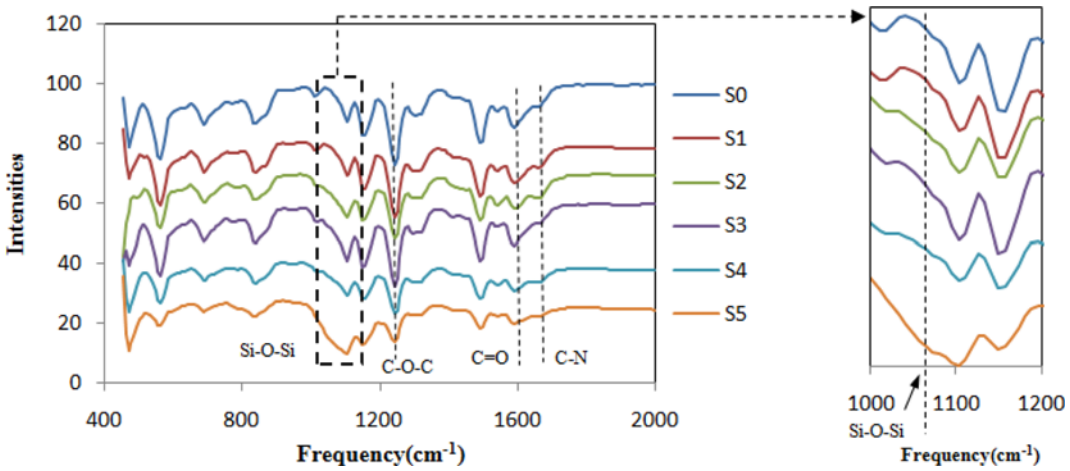

Fig. 4. ATR-FTIR spectra of PA and modified silica/PA membranes.

clearly present the primary amide (C=O) at 1,658 cm^{-1} and amide II (C-N) band at 1,560 cm^{-1} [28]. C-O-C stretching at about 1,245 cm^{-1} and CH_3-C-CH_3 stretching are assigned to the characteristic of polysulfone bands in sub-layer. The Si-O-Si peaks at 1,064 cm^{-1} confirmed the silica bands existing on the membrane surface, which probably represent overlapping with other peaks [1]. As indicated in Fig. 4, the Si-O-Si band intensity of the samples grows with increasing silica content. The ATR-IR spectrum of nanocomposite membranes shows the weakly increase of the peak intensity at 1,450 cm^{-1} and 1,369 cm^{-1} assigned to the CH and the CH_3 stretching, respectively, and 877 cm^{-1} is the characteristic of (=C-H) stretching of oleic acid. This band does not appear in the IR spectrum of neat polyamide. Upon the increasing nanosilica to membranes, the characteristic bands of (=C-H) at 850-900 cm^{-1} appeared weakly in the spectra of nanocomposite membranes, but this is not clearly distinguishable for S1 and S2. It indicates the interaction between C=C double bond of oleic acid with carboxyl group of TMC that is schematically depicted in Fig. 5. The (=C-H) stretching intensity increases for higher OA-modified silica content membrane due to agglomeration of nanoparticles and decrease of the interaction.

From the intensities of the 1,658 cm^{-1} band, the thickness of polyamide film over PSf sub-layer is calculated according to Eq. (1). The calculated thicknesses of polyamide films (t) are presented in Table 2. The low silica-containing polyamide film (sample S2) thickness is nearly the same as the neat polyamide film (S0); however

Table 2. Characteristics of nanocomposite membranes with different nano silica content

Sample	L_p (μm/MPa s)[a]	r_p (nm)[b]	t (nm)[c]
S0	2.5	0.345	61
S1	2.7	0.336	62
S2	2.7	0.319	84
S3	3.1	0.365	113
S4	4.3	0.413	151
S5	6.8	0.476	171

[a]Pure water permeability
[b]Radii of polyamide pores
[c]Thickness of polyamide layer

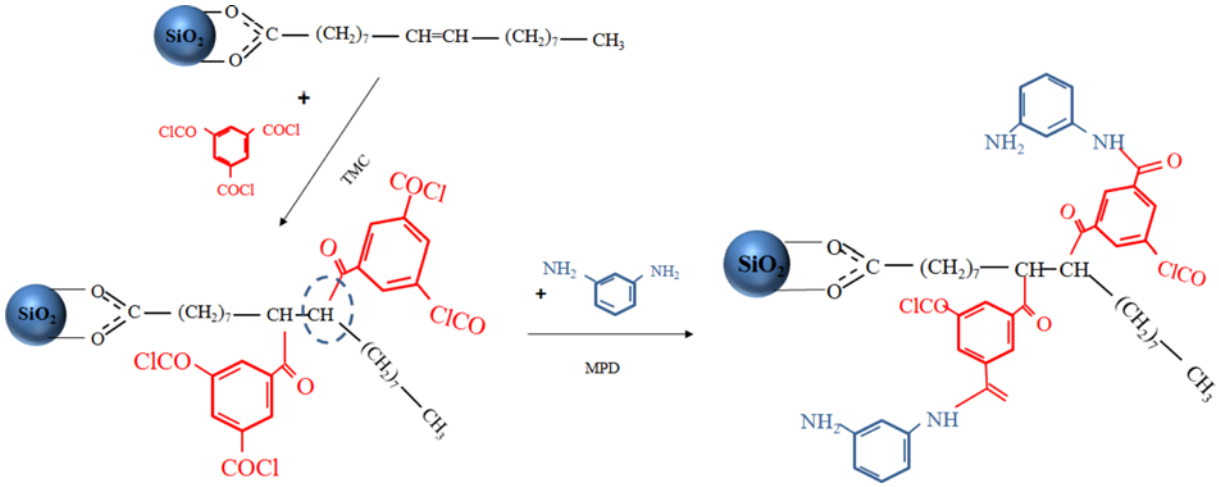

Fig. 5. The suggested reaction between OA- modified SiO_2 and TMC during polymerization of polyamide.

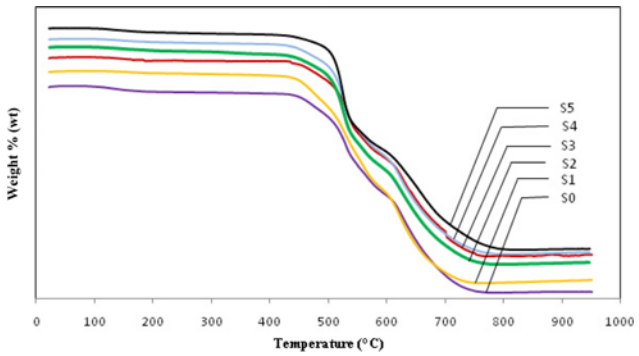

Fig. 6. TGA of neat PA and nanocomposite membranes. The curves have been shifted in vertical direction.

for higher silica-containing membranes (S3, S4 and S5), the film thickness is raised by excess silica, while the thickness of S5 is more than twice the thickness of S0. The ATR mode offers the possibility of concentration on a micron-thin layer, which makes it a suitable tool for studying the active layer thickness of composite membranes [16]. A_0 and A_t were estimated from ATR-FTIR data for C-C band of PSf and C-N polyamide stretch, respectively. According to Eq. (2), d_p is calculated about 1.156 μm.

The thermal stability of neat polyamide and prepared nanocomposite membranes is illustrated in Fig. 6. The decomposition range is about 528 °C to 650 °C for all samples. The initial region appeared from 50 to 200 °C with about 3% weight loss for all samples, which can be assigned to the evaporation of residual organic solvent and water after drying. TGA curves analysis suggests two major weight-loss regions, which is consistent with the results obtained by other researchers for polyamides [29,30]. The first decomposition begins at 528 °C for neat PA and in the range of 528 °C to 534 °C for S0 to S5 samples, whereby the main mass loss occurred in the materials. In the second region, the char that was formed from the earlier stage experienced continuous oxidative degradation [31]. The weight loss of lower nano silica content membranes is similar to neat polyamide. In the higher nano silica content membranes (S4 and S5), the range of decomposition temperature is enhanced. One possible explanation for this phenomenon is the strength of the interaction between the filler and the polymer during the polymerization, which is confirmed by FTIR test. The mass of residue is related to the nano silica content of membrane and increases with increasing silica loading (Table 3).

Table 3. TGA characteristics of the samples

Sample	Initial stage temperature (°C)	Decomposition stage temperature (°C)	Residue (wt%)
S0	131	452-529	8.7
S1	132	483-528	10.1
S2	141	489-531	10.9
S3	150	483-534	11.9
S4	152	484-534	14.2
S5	164	490-534	14.4

The surface morphology and cross section of PSf support membrane are displayed by SEM micrographs in Fig. 7. The neat PSf support membrane shows a featureless and smooth morphology of the surface. After interfacial polymerization onto PSf support membrane, the morphology of the top layer of PA is dense, rough and ridge-valley or leaf-like in shape. Fig. 8 presents the surface morphology of nanocomposite membranes as a function of nano-silica percentage. With the addition of modified silica nano particles, the surface microstructure of the samples is smoother for low silica content membranes. Clearly, the higher silica content samples have a rather rough surface morphology. As shown in the figure, a leaf-like structure is visible on the surface of S0 to S3, while S4 tends to a nodular surface structure. The presence of nano silica in the organic phase may enhance the miscibility of aqueous and organic phase during polymerization and ease of diffusivity of the MPD molecules in organic solution. However, by increasing the amount of nano silica, the agglomeration of particles has occurred, which can disturb the formation of polyamide film on the saturated support. This leads to the low formation of leaf-like folds of PA, which can be easily recognized in Fig. 8. Although the hydrophobic oleic acid on the surface of particles improves the dispersive capacity of nanoparticles in the organic solvent, because SiO_2 nanoparticles are very active to absorb OH, the groups of OH on the surface of the nanoparticles cannot be replaced with OA completely [20]. Therefore, the OH groups which remain on the

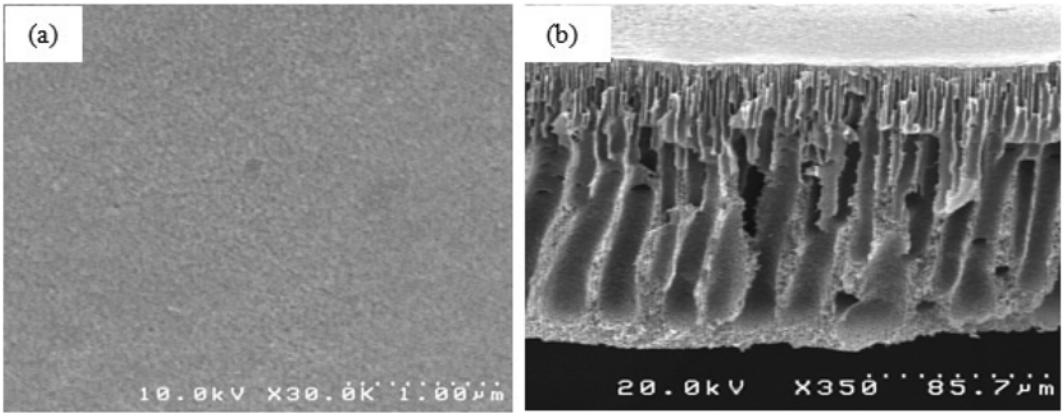

Fig. 7. SEM picture of: (a) surface and (b) cross section of PSf support.

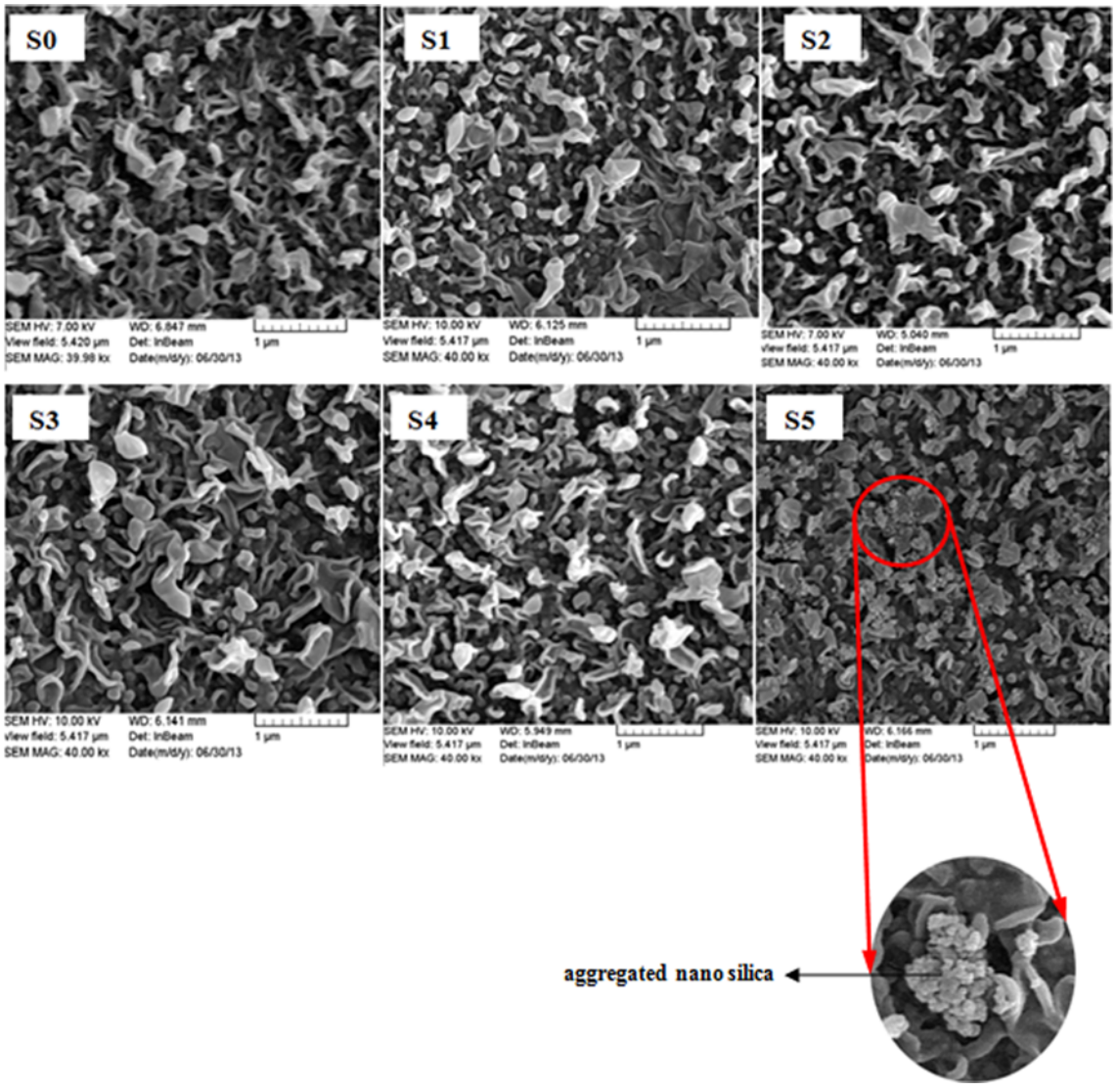

Fig. 8. FESEM images of TFC and TFN membranes.

surface of nanoparticles make them apt to aggregate in high silica concentration.

Fig. 9 shows cross sections of three different nanocomposite membranes. The layers of the membranes with different osmium tetroxide content are clearly recognizable in this figure. The images show the relatively rough ridge and valley structure characteristic of polyamide as confirmed by FESEM images. These prepared samples have a heterogeneous surface and various thicknesses. The protrusions at the surface of neat PA membrane are wormlike sharp-tip shapes, whereas the TFN membranes are almost similar to oval knoll of barrows. In this regard, similar findings can be found in literature [32]. According to Fig. 9(a), the total thickness of the neat PA membrane active layer can be estimated to be about 100 nm. By incorporating silica particles into PA selective layer, the thickness of PA increases, and this increase depends on the silica content. This result is consistent with the Jadav and Singh [1] study, in which they used the ATR-FTIR test for the evaluation of the thickness of silica/PA nanocomposite membranes. The thickness of low content silica layer (sample S2) is nearly the same as neat PA membrane, but the thickness of high silica content polyamide (sample S4) is about 190 nm. As indicated in the TEM pictures, the polyamide layer is not completely dense, and sporadic holes appear somewhere in the layer. Nevertheless, the polyamide has an ultra-thin inner layer, which seems dense and without any pores. The boundary between the two layers (dark and bright parts of membrane) corresponds to the dense barrier. The red circles in the PA layer are drawn around features believed to be silica nanoparticles.

The surface roughness of the samples was characterized by AFM. AFM measurements were performed on tapping mode, which is appropriate for soft polymers [15]. Typical 3D images of the surface of samples in 10 μm×10 μm frame are shown in Fig. 10. This clearly shows the heterogeneity of membrane surface with familiar ridge-valley morphology of PA membranes. Surface roughness (S_a and S_q) of samples is given in Table 4.

The roughness plays an important role in membrane performance, in that increase of roughness enhances the permeate flux; How-

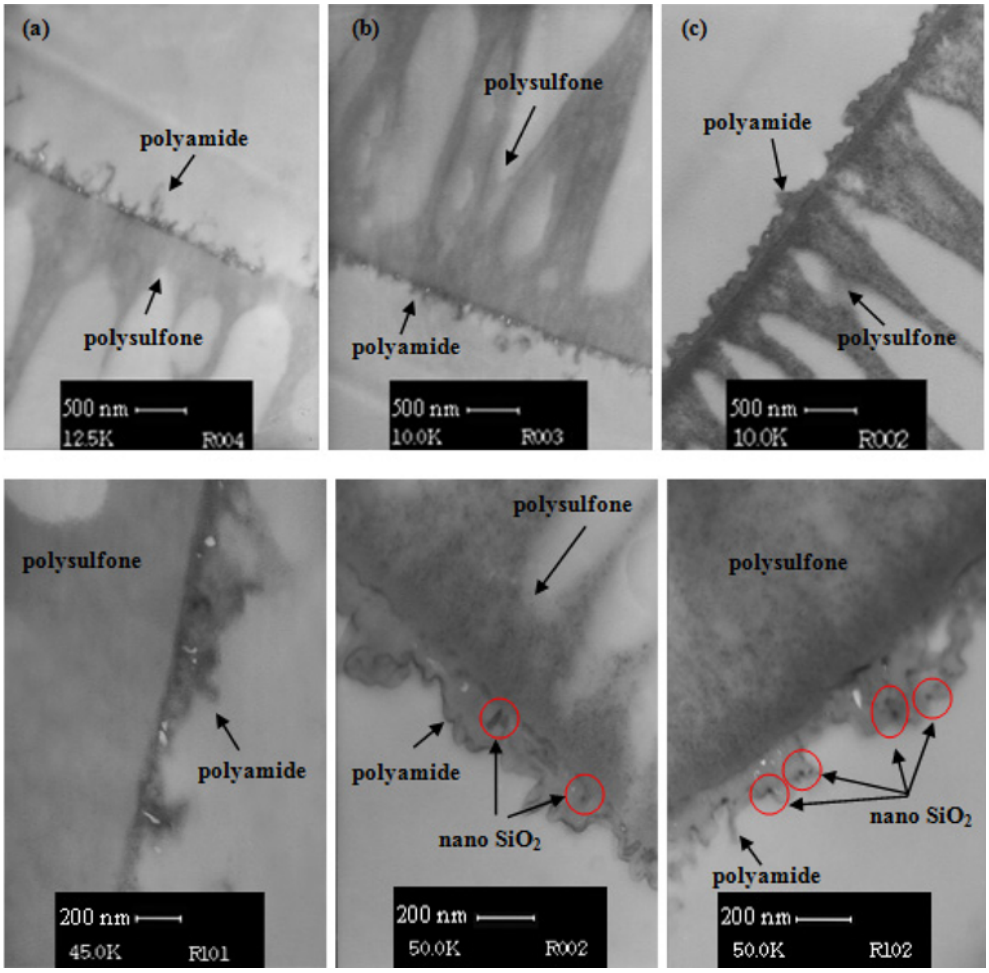

Fig. 9. TEM images of membranes (a) neat PA, (b) S2 and (c) S4.

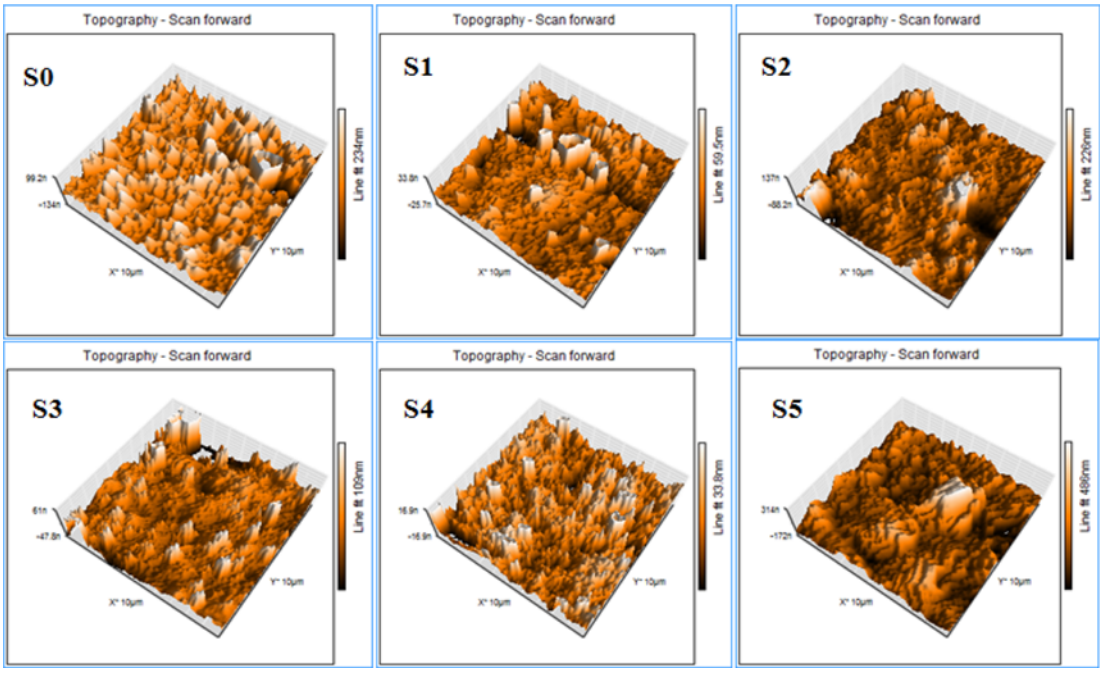

Fig. 10. AFM topography of nanocomposite membranes.

Table 4. Surface roughness and contact angle of nanocomposite membranes

Sample	S_a (nm)[a]	S_q (nm)[b]	Contact angle (degree)
S0	25.4	35.5	66.5
S1	23.6	32.6	53.3
S2	10.5	18.9	52.8
S3	13.6	23.6	47.3
S4	29.1	39.5	52.2
S5	55.2	73.5	56.4

[a]Average arithmetic roughness
[b]The root mean square roughness or RMS

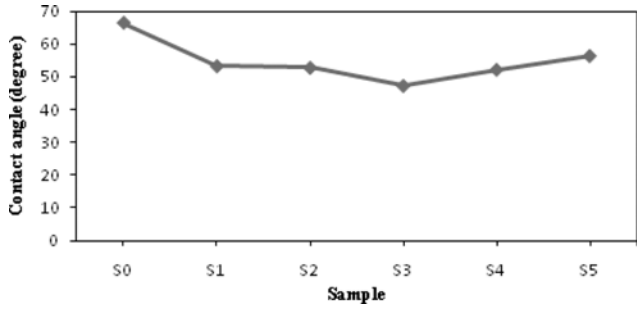

Fig. 11. Contact angle of OA-modified silica/PA membranes.

ever, it has often caused fouling due to particle trapping in the valleys. As reported in literature, when nanoparticle loading increases, TFN membranes become smoother [15]. The low-silica content membranes depicted in Fig. 10, show a smoother surface (32.6 nm and 18.9 nm) with fewer peaks compared to neat PA. This study revealed that the roughness is decreased by silica adding in low content, but after a specific concentration, the roughness increases with increase of silica loading. This behavior can be explained by nano silica agglomeration on the PA surface changing the membrane morphology and obtaining rougher surface as the S5 had the highest roughness, about 73.5 nm. The contact angle of synthesized membrane is plotted in Fig. 11. The contact angle of neat polyamide is about 66.5°. As the modified nano silica was added to polyamide, contact angle decreased to minimum 47.3° for the S3 sample. By adding further nano silica, fewer hydrophilic membranes (S4 and S5) with higher contact angle were produced. In general, adding nano silica to polymer increases the hydrophilicity of membrane surface, which leads to improvement in the water permeability and reduces fouling. But Surface modification of the silica particles with organic modifiers can decrease the amount of hydroxyl groups on the silica surface. Consequently, the aggregation of extra modified particles with hydrophobic groups on the surface reduces the hydrophilicity of the membrane, and finally increases the contact angle.

3. Membrane Performance in a Cross-flow Setup

The pure water flux of nanocomposite membranes for both modified and unmodified silica is shown in Fig. 12. The pure water flux in all cases of both series was enhanced by increasing the amount of nano particles. However, OA-modified silica/PA membranes flux was a little lower than that of unmodified silica/PA membranes.

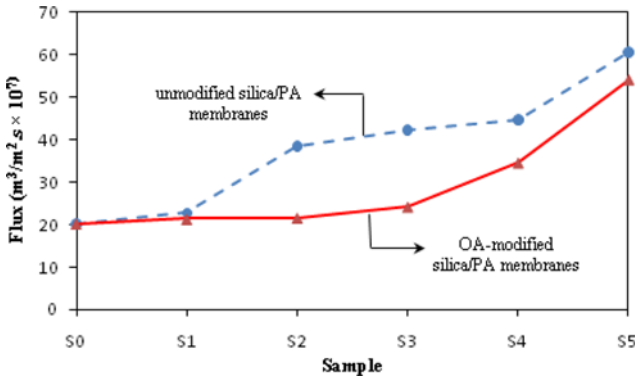

Fig. 12. Pure water flux of unmodified and OA-modified silica/PA membranes (T=25 °C, P=0.8 MPa).

It can be attributed to the role of COOH groups on the surface of silica that decreases the hydrophilicity of prepared TFN membrane. However, the permeability of OA-modified silica/PA membranes has been improved from 2.5 (μm/MPa s) for S0 to 6.8 for S5 as presented in Table 2. The pure water permeability of OA-modified silica/PA membranes correlates most strongly with hydrophilicity but not with roughness. The permeability of sample S2 with the smoothest surface (18.9 nm) is much higher than S0 with a more rough surface (35.5) but lower than S5 with the highest surface roughness (73.5 nm). Ghosh et al. [6] showed that the leaf-like folds on the membrane surface do not contribute directly to the permeation and only increased the contact area. Pore size of the PA layer is another effective parameter. The r_p for samples S1 and S2 was decreased compared to S0 (Table 2), so it can be said that their rejection enhanced. In addition, the permeate flux of polyamide composite membrane has been reported to be influenced by the thickness of thin barrier layer [6]. The membranes prepared in this study showed higher flux despite increasing thickness due to increased silica loading. Increase in thickness of barrier layer should increase the mass transfer resistant factor. If thicker layer has larger pores, it is clear that the total resistance decreases, and thereby permeate flux improves. On the other hand, permeate flux depends on hydrophilicity and porosity of the polyamide layer more significantly than other parameters such as film thickness or roughness. Salt rejection for $MgSO_4$ separation is presented in Fig. 13. In this figure,

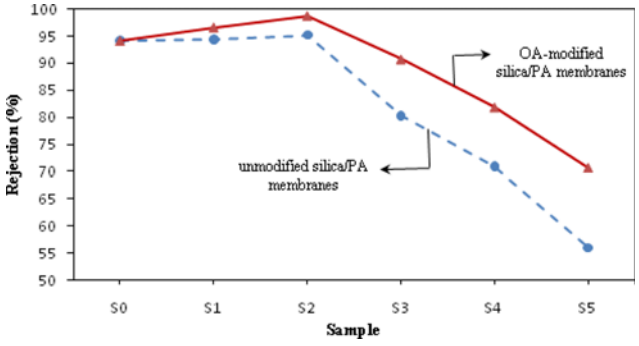

Fig. 13. $MgSO_4$ rejection of unmodified and OA-modified silica/PA membranes (T=25 °C, P=0.8 MPa).

the variation of rejection vs. various loading of nano silica is shown for both modified and unmodified nanocomposite membrane series. The neat PA rejection is about 94 percent. Only low-silica containing samples S1 and S2 exhibited higher rejection than neat PA membrane for both series. Among the prepared samples, S2 showed the best rejection, about 98.7 and 95.2 for modified and unmodified nanocomposite membrane, respectively; however, the rejection was decreased for high-silica loading samples (S3-S5). Singh and Aswal [9] studied the interaction between silica particles and PA layer by the small angle neutron scattering (SANS) technique. They found that for low containing silica nanocomposite membranes, the surface of silica particles interacts well with the polyamide chains, but this interaction was reduced for TFN samples with excess silica [9]. This comes from the fact that at higher loading content of silica, the phase separation exists by aggregated nano particles, which in turn reduces the PA crosslinking reaction significantly. In this case, more porous TFN is obtained. The size exclusion is very important and a well-known mechanism for the solute retention in nanofiltration membranes. The rejection of solutes governed by size exclusion from a nanofiltration membrane strongly depends on the membrane pore radii. To ascertain the influence of porous structure of silica/PA membrane skin on the rejection, the pore size (r_p) of modified nanocomposite membranes is displayed in Table 2. Results show an inverse relation between pore size and rejection as smaller pore size causes superior salt rejection (Fig. 13, Table 2). The average r_p for neat polyamide membrane is about 0.345 nm, and it is nearly the same of Mg^{2+} stokes radii (0.341 nm [33]). The r_p for S1 and S2 was decreased up to 0.319 nm and for both of them was smaller than Mg^{2+}. Whereas, the pore size of other samples (S3 to S5) increased up to 0.476 nm due to the particles agglomeration. These data can be used to justify the experimentally determined membrane rejections of $MgSO_4$ as presented in Fig. 13. In all samples, the rejections of OA-modified silica/PA membranes were higher than unmodified ones. Also as an interesting finding, the difference between rejections of the modified and unmodified TFN samples increased with silica loading. This can be explained by better affinity between modified silica consisting of COOH group and polymer chain compared to unmodified nano silica. In other words, functional groups of modified silica improve the crosslinking between polymer chains and cause a dense PA layer to form.

CONCLUSION

Oleic acid-functionalized silica nanoparticles were successfully prepared, characterized and incorporated into polyamide matrix to tailor the membrane structure and performance of TFN membranes for desalination. The silica nanoparticles were modified to provide COOH functionalized groups on the silica surface in order to increase interaction between nanoparticles and polymer matrix. Polyamide nanocomposite membranes were prepared via interfacial polymerization by dispersing the different loading of nanoparticles in TMC solution. The addition of modified silica to polyamide matrix caused hydrophilicity and water flux of TFN membranes to increase. FESEM and AFM surface images of TFC and TFN membranes showed initially a surface roughness, which was reduced by adding of modified silica, and then increased by further increasing of silica amount. The behavior of OA-modified silica/PA membranes in salt rejection and water flux experiments was compared to unmodified silica/PA membranes. The results confirmed that OA-modified silica membranes demonstrated higher salt rejection but lower water flux than unmodified ones.

ACKNOWLEDGEMENT

We gratefully acknowledge the financial support of this study by the Iran National Science Foundation (INSF). We also thank the chemical engineering laboratory of Ferdowsi University of Mashhad for TGA experiment.

REFERENCES

1. G. L. Jadav and P. S. Singh, *J. Membr. Sci*., **328**, 257 (2009).
2. M. Fathizadeh, A. Aroujalian and A. Raisi, *Desalination*, **284**, 32 (2012).
3. A. K. Ghosh and E. M. V. Hoek, *J. Membr. Sci*., **336**, 140 (2009).
4. P. S. Singh, A. P. Rao, P. Ray, A. Bhattacharya, K. Singh, N. K. Saha and A. V. R. Reddy, *Desalination*, **282**, 78 (2011).
5. W. Xie, G. M. Geise, B. D. Freeman, H. S. Lee, G. Byun and J. E. McGrath, *J. Membr. Sci*., **403-404**, 152 (2012).
6. A. K. Ghosh, B. H. Jeong, X. Huang and E. M. V. Hoek, *J. Membr. Sci*., **311**, 34 (2008).
7. J. Lee, C. M. Doherty, A. J. Hill and S. E. Kentish, *J. Membr. Sci.*, **425-426**, 217 (2013).
8. P. B. Kosaraju and K. K. Sirkar, *J. Membr. Sci*., **321**, 155 (2008).
9. P. S. Singh and V. K. Aswal, *J. Colloid Interface Sci*., **326**, 176 (2008).
10. T. A. Saleh and V. K. Gupta, *Sep. Purif. Technol*., **89**, 245 (2012).
11. C. H. Lee, W. Xie, D. VanHouten, J. E. McGrath, B. D. Freeman, J. Spano, S. Wi, C. H. Park and Y. M. Lee, *J. Membr. Sci.*, **392**, 157 (2012).
12. T. Bae, I. Kim and T. Tak, *J. Membr. Sci.,* **275**, 1 (2006).
13. M. Alexandre and P. Dubois, *Mater. Sci. Eng*., **28**, 1 (2000).
14. G. L. Jadav and P. S. Singh, *J. Membr. Sci*., **328**, 257 (2009).
15. B. H. Jeong, E. M. V. Hoek, Y. Yan, A. Subramani, X. Huang, G. Hurwitz, A. K. Ghosh and A. Jawor, *J. Membr. Sci*., **294**, 1 (2007).
16. C. Kong, A. koushima, T. Kamada, T. Shintani, M. Kanezashi, T. Yoshioka and T. Tsuru, *J. Membr. Sci*., **366**, 382 (2011).
17. M. T. M. Pendergast, A. K. Ghosh and E. M. V. Hoek, *Desalination*, **308**, 180 (2011).
18. L. Jin, W. Shi, S. Yu, X. Yi, N. Sun, C. Ma and Y. Liu, *Desalination*, **298**, 34 (2012).
19. J. Kim and B. Van der Bruggen, *Envi. Pollut*., **158**, 2335 (2010).
20. Z. Li and Y. Zhu, *Appl. Surf. Sci*., **211**, 315 (2003).
21. E. S. Kim and B. Deng, *J. Membr. Sci*., **375**, 46 (2011).
22. S. Mallakpour and A. Barati, *Prog. Org. Coat.*, **71**, 391 (2011).
23. H. Namazi and H. Ahmadi, *J. Power Sources*, **196**, 2573 (2011).
24. R. P. Bagwe, L. R. Hilliard and W. Tan, *Langmuir*, **22**, 4357 (2006).
25. J. W. Goodwin, R. S. Harbron and P. A. Reynolds, *Colloid Polym. Sci.,* **268**, 766 (1990).
26. M. Z. Rong, M. Q. Zhang and W. H. Ruan, *Mater. Sci. Technol*., **22**, 787 (2006).
27. V. Freger, A. Bottino, G. Capannelli, M. Perry, V. Gitis and S. Belfer, *J. Membr. Sci.,* **256**, 134 (2005).

28. C. Y. Tang, Y. N. Kwon and J. O. Leckie, *Desalination*, **242**, 149 (2009).
29. S. C. Tjong and S. P. Bao, *J. Polym. Sci.*, **42**, 2878 (2004).
30. B. N. Jang and C. A. Wilkie, *Polymer*, **46**, 9702 (2005).
31. X. Zhang and L. S. Loo, *Polymer*, **50**, 2643 (2009).
32. F. A. Pacheco, I. Pinnau, M. Reinhard and J. O. Leckie, *J. Membr. Sci.*, **358**, 51 (2010).
33. A. A. Hussain, M. E. E. Abashar and I. S. Al-Mutaz, *Desalination*, **214**, 150 (2007).